Journal of the mechanical behavior of biomedical materials 71 (2017) 279–285

Contents lists available at ScienceDirect

Journal of the Mechanical Behavior of Biomedical Materials

journal homepage: www.elsevier.com/locate/jmbbm

Elastic modulus varies along the bovine femur

Sabah Nobakhti[a,*,1], Orestis L. Katsamenis[d], Nizar Zaarour[b], Georges Limbert[a], Philipp J. Thurner[a,c]

[a] Bioengineering Science Research Group, Engineering Sciences, Faculty of Engineering and the Environment, University of Southampton, Southampton SO17 1BJ, UK
[b] Supply Chain and Information Management Group, D'Amore-McKim School of Business, Northeastern University, 360 Huntington Avenue, Boston, MA 02115, USA
[c] Institute of Lightweight Design and Structural Biomechanics, Vienna University of Technology, Getreidemarkt 9, A-1060 Vienna, Austria
[d] μ-VIS X-Ray Imaging Centre, Faculty of Engineering and the Environment, University of Southampton, Southampton SO17 1BJ, UK

ARTICLE INFO

Keywords:
Cortical bone mechanics
Micro-computed tomography
Micro-CT gray-level to elastic modulus conversion

ABSTRACT

Bone is a heterogeneous material and its mechanical properties vary within the body. Variations in the mechanical response of different bone samples taken from the body cannot be fully explained by only looking at local compositional information at the tissue level. Due to different states of the stress within bones, one might expect that mechanical properties change over the length of a bone; this has not been a matter of systematic research in previous studies. In this study, the distribution of the tissue elastic modulus along the bovine femur is investigated using three-point bending tests. Two bovine femora were split to seven and eight blocks from proximal to distal metaphysis, respectively and twenty beam shaped bone samples were extracted and tested from each block. Based on our findings, the longitudinal elastic modulus follows a gradient pattern along the bovine femur as it increases along the bone from the proximal metaphysis to mid-diaphysis and then decreases toward the distal metaphysis again. Considering long bones to be subjected to bending loads, this mechanism alters the bone structure to support load in the regions where it is needed; similar as outlined by Wolff's law. In another part of this study, microfocus X-ray computed tomography (μCT) was found unable to predict the same trend of changes for the elastic modulus via image-based or density-based elastic moduli calculations. This is insofar important as conventional finite element models of bone are often directly shaped from μCT data. Based on our findings, it seems that current computed tomography based finite element models generated in this manner may not adequately capture the local variation of material behavior of bone tissue, but this may be improved by considering the changes of the elastic modulus along the femur.

1. Introduction

Bone is a smart structure/material, which is capable of adapting to applied forces (Wolff, 1892), while achieving an optimum and minimal-weighted structure with high load bearing capacity. In general, bone is not subjected to one loading case but to various loading conditions. Considering long bones for instance, human femur experiences complex bending, torsion and compression loading regimes during a gait cycle (Duda et al., 1998; Edwards et al., 2008). As bone adapts to mechanical loads throughout life (Wolff, 1892), it is expected that stronger or weaker regions form in mature skeleton due to habitual loading, and are optimized for the loads experienced. While several previous studies have reported differences in stiffness, ultimate strength and apparent density for various anatomical locations within the long bones (Atkinson and Weatherell, 1967; Les et al., 1997; Espinoza Orías et al., 2009; Rantalainen et al., 2011; Rohrbach et al., 2012), a systematic approach to characterize the degree of heterogeneity of micro-level mechanical properties along the bone seems to be missing in literature. From a structural point of view, bone is thicker where it has to withstand higher stresses. We hypothesize that the bone material also adapts to the condition of high stress in those regions and therefore, the elastic modulus is positively correlated to cortical bone thickness in bovine femur. As thickness varies in long bones, we hypothesize that there is a correlation between the elastic modulus and position along the bovine femur, with elevated moduli at mid-shaft.

The heterogeneity of the elastic modulus in bone is a key feature

* Corresponding author.
E-mail addresses: Nobakhti.s@husky.neu.edu (S. Nobakhti), O.Katsamenis@soton.ac.uk (O.L. Katsamenis), N.zaarour@northeastern.edu (N. Zaarour), G.limbert@soton.ac.uk (G. Limbert), Philipp.thurner@tuwien.ac.at (P.J. Thurner).
[1] Present address: Department of Mechanical and Industrial Engineering, Northeastern University, 360 Huntington Avenue, Boston, MA 02115, USA.

http://dx.doi.org/10.1016/j.jmbbm.2017.03.021
Received 17 August 2016; Received in revised form 5 March 2017; Accepted 25 March 2017
Available online 27 March 2017
1751-6161/

and many models try to take that into account in finite element (FE) analysis of bone tissue. FE models are extensively used in the study of the mechanics of bone and artificial implants e.g. (Duda et al., 1998; Polgar et al., 2003; Shahar et al., 2003; Poelert et al., 2012). In conventional FE modeling of the bone however, the regional dependency of mechanical properties is neglected and bone is assumed to be a homogeneous isotropic material (Polgar et al., 2003; Shahar et al., 2003). A more sophisticated approach in FE modelling is to extract the mechanical properties of bone from computed tomography (CT) data, converting local grey level numbers to bone mineral density (BMD) and subsequently to a local elastic modulus (Crawford et al., 2003a, 2003b; Taddei et al., 2006; Poelert et al., 2012). Whether the elastic modulus is positively related to bone mineral density in μCT measurements is still not clear. It has been previously shown in some studies that bone becomes stiffer with an increase in the degree of mineralization (Follet et al., 2004; Wagner et al., 2011). Some other studies, however, reported only a weak correlation between the bone mineral density and the elastic modulus (such as Rho et al., 1995). In this paper, we compared the bone mineral density to the elastic modulus to search for the validity of their relation in bovine bone. We hypothesize that the elastic modulus is not correlated to bone mineral density in bovine femur.

As an alternative to bone mineral density, we propose that complementary approaches to CT-based calculations can be developed based on location dependency of the elastic modulus in long bones, to precisely map the local elastic properties of the bone in finite element models. After proper calibration of the method for each case, an accurate estimation of the elastic modulus may be found for long bones. In this study, we report results from miniature three-point bending experiments on samples taken at regular intervals along the long axis of two bovine femora. Through comparison with μCT data, we can compare CT predicted longitudinal elastic modulus with the actual measurements. From the findings of our experiments, we propose that complementary empiric laws to the current CT-based approaches can more accurately predict the local longitudinal elastic modulus along the bovine femur.

2. Materials and methods

Two bovine femora were tested in this study. Femur-1 was tested to investigate the correlation of the elastic modulus with position along the long axis of the bone, cortical bone thickness and for comparison with local elastic moduli predicted by μCT. Three-point bending experiments were repeated on femur-2 to check if the relationship found for femur-1 can predict the elastic modulus for other bones. Bovine femora were obtained from local meat wholesalers and stored at −20 °C until scanning and sample preparation.

2.1. Microfocus X-ray computed tomography (μCT)

μCT imaging on femur-1 was performed at the University of Southampton μ-VIS X-Ray imaging center using a Custom 225 kVp Nikon/Metris HMX ST scanner (Nikon Metrology, Brighton, MI, US) equipped with a 2000×2000 pixel flat panel detector. To ensure sufficient flux a W target was selected, the voltage was set at 200 kV and no pre-filtration was used. The current was set at 29 μA (5.8 W), and the source to detector distance was 672.56 mm, resulting in an isotropic pixel resolution of 59.1 μm in x, y and z directions for the scan. The femur was placed upright in a shielded Perspex tube and positioned onto the rotation stage, so that the long axis of the bone coincided with the stage's center of rotation (CoR). The position of the specimen and the distance from the X-Ray source were such that ensured the whole width and depth of the bone remained within the field of view during the full 360 degree rotation. To cover the whole specimen at the aforementioned resolution, we divided the imaging volume into three sub-volumes (i.e. bottom-, middle- and top-raster) and each raster was scanned separately keeping imaging conditions constant. In more detail: 3142 projections were taken over the 360-degree rotation (Angular Step=0.1146 deg), with 4 frames per projection being averaged in order to improve the signal to noise ratio. Exposure time of each projection was 354 ms and the gain was set to 30 dB. Once the scans were complete, the reconstructions parameters were defined using CTPro software (Nikon Metrology, Brighton, MI, US) and reconstructed in CTAgent (Nikon Metrology, Brighton, MI, US) reconstruction software, which uses a filtered back-projection algorithm. The output volume data were scaled to Hounsfield units using a known density phantom (in our case water), following Nikon's recommendations. The three calibrated volumes were then concatenated into a single volume using Fiji/ImageJ (National Institute of Health, Bethesda, MD, US) and orthogonal central cross-sections along the XZ and YZ planes (Z being in line with bone's long axis) were exported for further analysis. Thickness of the bone cortex in each anatomical location within the blocks was measured in several sites from the μCT data and in MATLAB (The Math Works, Natick, MA, US). On each cross-section and at approximately the middle of the bone cortex, a line profile (width 10 pixels) was measured using Fiji's profile tool (Fig. 1). This allowed averaging the measured gray value, over a larger bone area, reducing possible bias due to local pixel variations and beam hardening effects.

Calibrated Hounsfield units (HU) along each profile were converted to the bone mineral density (BMD) using Eq. 1 (Schneider et al., 1996) and consequently to the elastic modulus (E) using Eq. 2, the empirical relationship proposed by Rho et al. (1995).

$$BMD\ (g/cm^3) = 0.0007 \times HU + 0.3489 \quad (1)$$

$$E\ (GPa) = 9.11 \times BMD^{1.326}\ (g/cm^3) \quad (2)$$

2.2. Sample preparation

Femur-1 was cut along its longitudinal and perpendicular axes using a bandsaw (BG 200, Medoc, Logrono, Spain). The bone was then divided into 8 blocks along its longitudinal axis (block height= 2 cm), excluding the epiphyses. This configuration is shown in Fig. 2. Blocks 1

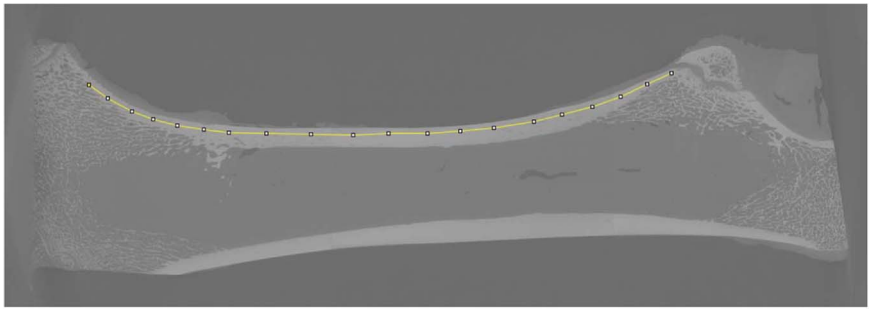

Fig. 1. - Line profile used to extract the CT graylevel number and mineral density from the anterior section of femur-1.

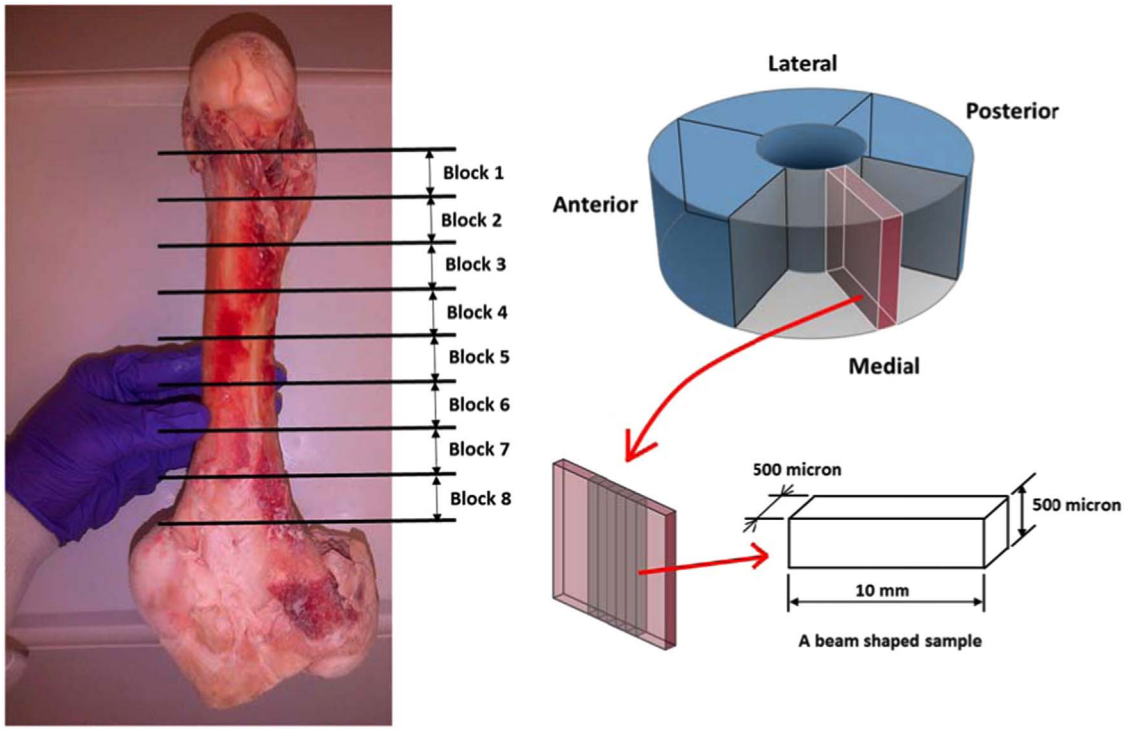

Fig. 2. - Left) femur-1 divided into 8 blocks of 2 cm height, Right) One sample block divided into four sections and representation of the bone plate extracted from each block. Five longitudinal beam shaped samples were made out of the bone plate for each quadrant in the block. Block height in femur-2 was 3 cm and each sample's length was approximately 15 mm and 10 mm for femur-1 and femur-2 specimens, respectively.

and 8 corresponded to the location of proximal and distal metaphyses, respectively. Femur-2 was divided into 7 blocks in a similar manner (block height= 3 cm). Anterior, posterior, medial and lateral sectors of every block were separated for each bone.

The bone marrow in all the blocks was removed using a cold water jet, which was provided by connecting a plastic pipette tip to a plastic tube linked to a water tap. Cut bone pieces were kept in the Hank's Buffered Salt Solution (HBSS) of pH≈7.4 throughout sample preparation and at temperature≈ 4 °C between individual preparation steps. Each block was then packed with gauze, soaked in HBSS and stored in sealed plastic bags at −20 °C. In order to prepare suitable cortical bone samples for three-point bending tests, a low speed saw (IsoMet, Buehler, 86 Lake Bluff, IL, USA) with a diamond wafering blade was used. Each bone block was cut in several steps to produce cortical beam shaped samples of approximate cross section 500 μm×500 μm as sketched in Fig. 2. Each beam shaped sample's length was approximately 15 mm and 10 mm for femur-1 and femur-2 specimens, respectively. To make the beams, a sheet of bone (thickness ~ 500 μm) was longitudinally cut (parallel to the bone longitudinal axis) in the endosteum-periosteum direction for each of the anatomical sectors in every block and from that sheet, five longitudinal cortical beam shaped samples (width ~ 500 μm) were collected such that samples were located beside each other in the main sheet of the bone and positioned approximately in the middle of the bone cortex (Fig. 2). 160 and 140 longitudinal cortical beam shaped samples were collected from femur-1 and femur-2, respectively.

2.3. Three-point bending experiments

Two three-point bending fixtures were used to test the samples extracted from each femur. Femur-1 specimens were tested in a three point bending fixture (span length 10 mm and roller radius 0.75 mm). To test femur-2 samples, a similar three point bending setup was used, designed based on the standard of American Society of Agricultural and Biological Engineers (ASABE) (Szabo et al., 2011). The span length for this fixture was 2 mm and the roller radius was 0.25 mm. A miniature load frame (ElectroForce3200, Bose, Eden Prairie, MN, USA) was used to perform the tests in displacement controlled mode with a displacement rate of 0.01 mm/s. A bath made of transparent plastic (polymethyl methacrylate) and glass, filled with HBSS (pH≈7.4), was used to ensure testing of bone samples in hydrated condition.

2.4. Data analysis

Load-displacement data were recorded by the mechanical testing system for every sample. To find the stiffness (load vs. displacement ratio), maximum slope of the linear region of each data set was computed using a custom MATLAB code (The Math Works, Natick, MA, US) consistently for every sample. Timoshenko beam theory was used to calculate the longitudinal elastic moduli of each sample. Based on Timoshenko beam formulation, elastic modulus for each sample can be estimated from the stiffness and geometrical measures (Gere and Timoshenko, 1991):

$$E = \left(\frac{P}{v}\right)\frac{L^3}{48I}\left(1 + \frac{24(1+v).\,I}{AkL^2}\right) \quad (3)$$

In Eq. (3) E corresponds to elastic modulus, (P/v) is the stiffness, I is second moment of area, v is Poisson's ratio taken as 1/3, A is cross-sectional area of each sample, L is sample length between lower bending supports and k is shear coefficient taken as 0.850 for a rectangular cross-section (Cowper, 1966). Elastic moduli of all five samples tested from each region (anterior, posterior, medial and lateral) for every block were then averaged to estimate the longitudinal elastic modulus in the anatomical locations for individual blocks. To calculate the cross-section and second moment of area for each specimen, an average of width and height of the samples measured by a digital caliper at three different locations was used.

2.5. Statistical analysis

Mean and standard deviation of the elastic moduli were computed for three-point bending and μCT based calculations along the bone. Hypothesis testing and confidence intervals were used to compare the findings of the two different methods. A regression model was used to investigate the correlation of the elastic modulus with the position along the bone and cortical bone thickness. In the model, ANOVA and two-tailed student t-tests were employed to search for the significance of the findings in normally distributed data with $p < 0.05$ in Microsoft Excel 2013 (Microsoft, WA, US) and Minitab 17 (Minitab Inc., PA, US) packages.

3. Results

3.1. Elastic modulus values computed from μCT are significantly different to ones obtained from three-point bending

The variation of the elastic moduli within each quadrant (anterior, posterior, medial and lateral) with position along the femur was obtained from μCT data and compared to three-point bending results as shown in Fig. 3 for femur-1 specimens. Hypothesis testing and confidence intervals analysis showed that the elastic modulus computed from CT is significantly different ($p < 0.05$) in every quadrant from the elastic modulus measurements in three-point bending tests, with lower values in three-point bending (Fig. 3). In a more generalized approach, the effect of quadrant was neglected from the analysis and three-point bending results were compared to CT-based calculations for the same bone as shown in Fig. 4. Only a very weak correlation ($R^2=0.03$, $p < 0.05$) was found between the elastic modulus calculated from CT density and three-point bending. For a complete list of the data from each technique please refer to Supplementary Materials, Table-1.

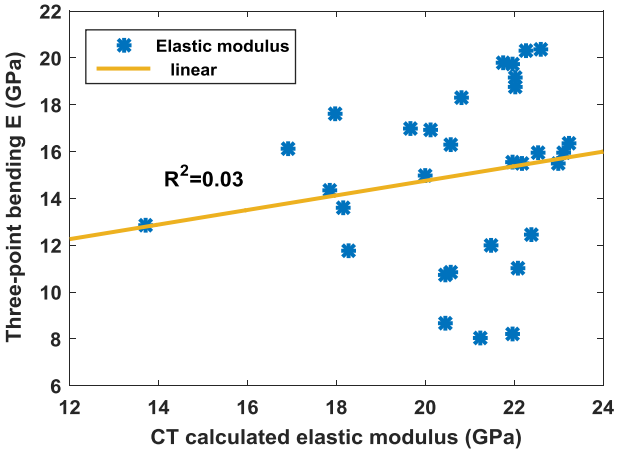

Fig. 4. - Correlation of the elastic modulus calculated from CT mineral density and the elastic modulus found in three-point bending tests is very weak ($R^2=0.03$, $p < 0.05$).

3.2. Prediction of the elastic modulus by position along the femur

To test if the position of the bone specimens from the proximal / distal end of the femur correlates to the longitudinal elastic modulus, we fitted a second order polynomial to elastic modulus values plotted

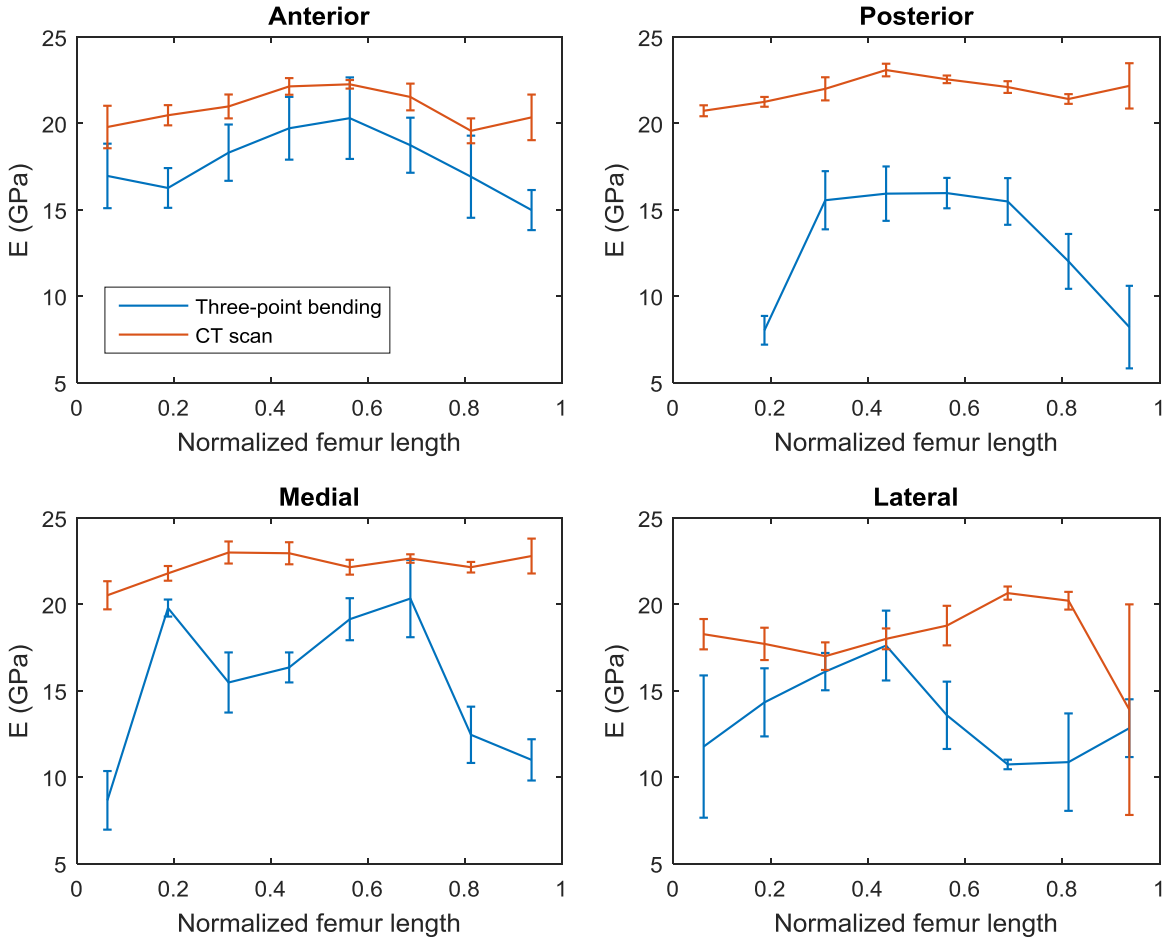

Fig. 3. - Comparing the elastic modulus computed from three-point bending and μCT for different quadrants along the femur-1. As shown, three-point bending results are significantly lower than CT predictions.

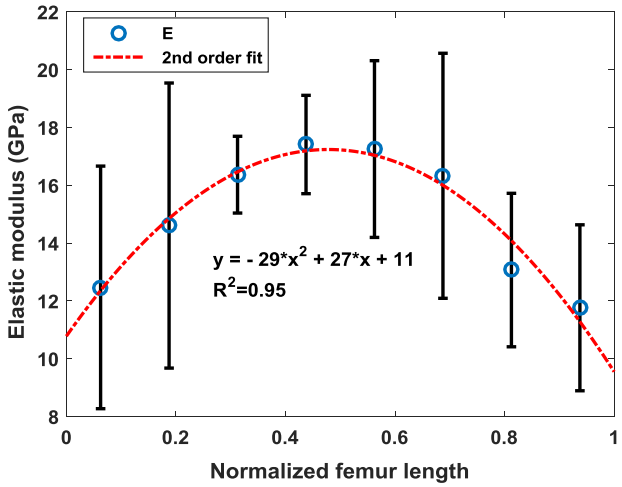

Fig. 5. - Elastic modulus of three-point bending tests is strongly correlated to position along the axis of femur-1 (R^2=0.95, $p < 0.05$). Error bars show the standard deviation.

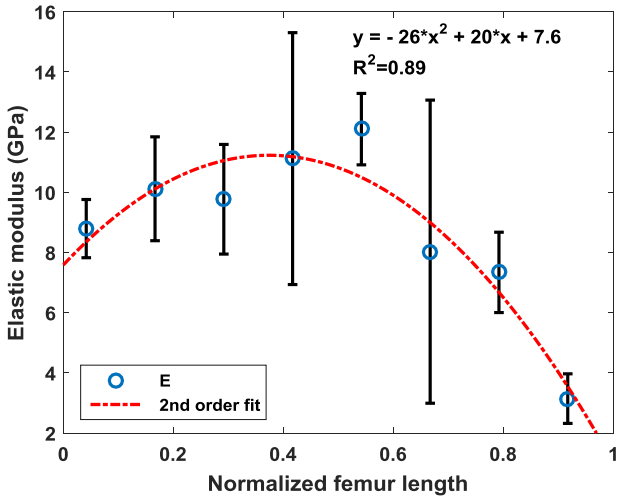

Fig. 6. - Elastic modulus of three-point bending tests is strongly correlated to position along the axis of femur-2 (R^2=0.89, $p < 0.05$). Error bars show the standard deviation.

vs. position along the femur-1 for each quadrant. We found strong correlations between the position along the bone and longitudinal elastic modulus for the anterior (R^2=0.79, $p < 0.05$) and posterior (R^2=0.92, $p < 0.05$) quadrants however, for medial (R^2=0.60, $p < 0.05$) and lateral (R^2=0.34, p=0.26) quadrants, these correlations were weaker or insignificant, respectively. In the next step, the elastic moduli data from all quadrants were pooled and the correlation of an average longitudinal elastic modulus of the samples within the block with regards to position along the bone was investigated. This was done to obtain overall insight into the variation of elastic modulus along the femur, despite the fact that there might be significant differences between some of the groups (58% when comparing elastic moduli values between various quadrants within each block, $p < 0.05$). Fig. 5 shows the correlation of normalized position along the femur and the averaged elastic modulus for each block. As shown, the longitudinal elastic modulus correlates with the position along the femur (R^2=0.95, $p < 0.05$) with higher values at the mid-diaphysis compared to the metaphysis.

The empirical relation found for femur-1 was then applied to femur-2 data. In a regression analysis, elastic modulus of femur-2 was significantly correlated to position along the bone (R^2=0.61, $P < 0.05$) using the formula found for femur-1. To find an exact correlation between the elastic modulus and position along the bone for femur-2, the same analysis as femur-1 was repeated. In this case, correlation of the elastic modulus and normalized position of samples along the bone was only significant in the anterior quadrant (R^2=0.93, $p < 0.05$) when fitting a second order polynomial to data. For posterior (R^2=0.35, p=0.32), medial (R^2=0.50, p=0.16) and lateral (R^2=0.21, p=0.63) quadrants however, position along the femur was not a good predictor for the elastic modulus. Similar to our approach for femur-1, correlation of the normalized position along the femur and the averaged elastic modulus of all quadrants in each block was investigated as shown in Fig. 6. Again, this was done to obtain overall insight into the variation of elastic modulus along the femur, despite the fact that there was significant differences between the elastic moduli of quadrants in some cases (36% when considering all combinations in each block, $p < 0.05$), similar to femur-1, there is a gradient trend for the elastic modulus along the femur with elevated values at mid-diaphysis which could be explained based on the normalized position of samples along the femur (R^2=0.89, $p < 0.05$).

3.3. Cortical bone thickness is not a good predictor for the elastic modulus

We further tested whether cortical bone thickness correlates to the longitudinal elastic modulus for different quadrants in femur-1 data. ANOVA regression analysis did not show any significant correlations between longitudinal elastic modulus and cortical bone thickness. We then performed a statistical analysis to see if the effect of quadrants could be neglected when reporting thickness and an averaged value for each block could be reported. In a two-tailed student t-test, 99% of p values were < 0.05 when considering the difference of cortex thickness in various quadrants of one block, indicating that thickness data are significantly different between the quadrants and cannot be averaged within a block. We then investigated the correlation of averaged cortex thickness and the averaged elastic modulus for every anatomical location within each block. As shown in Fig. 7, there is no significant correlation between the thickness and the elastic modulus (R^2=0.03, p=0.35).

4. Discussion

Inferring bone tissue level properties in FE models correctly is important for achieving quantitative results and for the potential predictive character of such models. This study provides evidence that the longitudinal elastic modulus of cortical bovine bone varies along the femur. Our data suggest that the mid-diaphysis section of bovine femur is stiffer compared to other parts of the bone; this is in agreement with Les et al. (1997) and Espinoza Orías et al. (2009) who found similar trends in the equine third metacarpal bone and

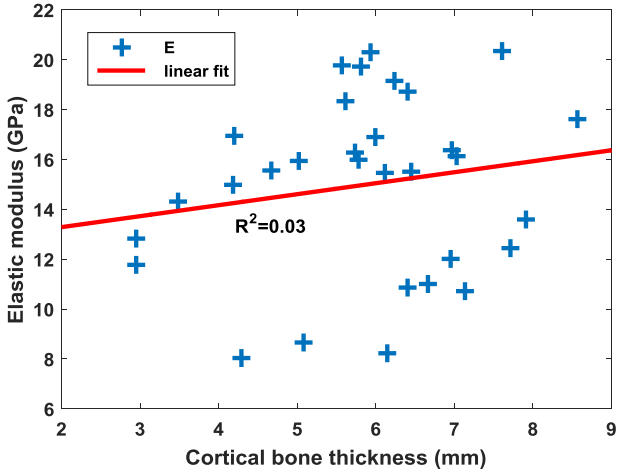

Fig. 7. - Correlation of cortical bone thickness and the elastic modulus for femur-1 is not significant (R^2=0.03, p=0.35).

human femur, respectively. Based on our findings, it is likely that similar gradient patterns of the elastic modulus exist along the axis of other long bones, which are subjected to bending loads. Oh and Harris (1978) studied the proximal human femur in a single limb stance phase of loading. They reported that tensile and compressive strains decrease from proximal to mid-diaphysis in all anatomical cortices of the bone transverse cross-sections. Bending loads on the bovine femur might result in larger strain variation along the bone compared to the human femur. The strain would then decrease along the same path as the bone due to translation of similar forces to areas with higher cross section and higher elastic modulus in bovine bone. The femur in mammals is normally subjected to bending loads as suggested by Polgar et al. (2003) and Shahar et al. (2003) and has a non-uniform strain distribution along the bone axis (Duda et al., 1998; Shahar et al., 2003; Polgar et al., 2003). Based on these observations, variations of the elastic modulus along the longitudinal axis of bovine femur seems sensible; extreme strains predicted in or around the mid-diaphysis in isotropic finite element models of the femur (Duda et al., 1998; Shahar et al., 2003; Polgar et al., 2003) indicate that the elevated elastic modulus in that region would enhance the bone structural integrity by reducing the actual strains formed in everyday activities. Previous reports as well as our findings, support the idea that cortical bone in general has its highest stiffness in the areas subjected to major loads. As previously noted by Wolff's law (Wolff, 1892), bone apposition occurs in regions subjected to "higher" stresses and bone resorption happens in areas subjected to "lower" stresses. Based on our findings, one may speculate that in addition to Wolff's law for bone adaptation in a geometrical or bone mass sense, a similar argument may be formulated with regards to the bone structure and its local properties, i.e. local bone stiffness can adapt as a response to experienced stresses – locations experiencing elevated stress will not only form more bone, but also bone tissue with elevated elastic modulus.

To date, probably the most common approach to assign heterogeneous material properties to finite element models of bone is the conversion of grey level numbers from computed tomography data into elastic modulus values. This conversion is usually achieved by power law relationships between the elastic modulus and density via calibrated Hounsfield units (Rho et al., 1995) or calibration via density phantoms. Such approaches surely are an advancement compared to isotropic homogeneous models. However, as reported by Rho et al. (1995) density alone in human femur leaves 30% of the variation of the elastic modulus unexplained in the longitudinal direction. Further, based on our findings, the power of μCT to provide accurate estimation of variations of the elastic modulus in long bones (from Eqs. 2–3) for computational models is rather limited, which is in agreement with Cuppone et al. (2004). We tested if a different power law can be established between the three-point bending elastic modulus and CT density based on the data for femur-1 however, the correlation ($E=11.256\times BMD^{0.4133}$, $R^2=0.018$) was very weak. This can be explained based on the fact that the elastic modulus is only predicted from the bone mineral density in μCT. In addition to the role of the local mineral concentration, mechanical properties of the bone at the tissue level are also affected by other microstructural and compositional features of bone.

In a similar study by Rohrbach et al. (2012), tissue level mineral density was found by synchrotron radiation microfocus computed tomography (SRμCT) and compared with the longitudinal elastic modulus in bone. Rohrbach et al. recorded elevated values of mineral density at mid-diaphysis of human femur similar to what we found for the elastic modulus variations along the bovine femur. They have reported a positive correlation for the longitudinal elastic modulus with position along the femur such that the elastic modulus decreases when moving from the proximal to distal part of the bone, different to our findings for bovine bone. However, the mineral density variations along the bone was not reflected in the same manner as the elastic modulus in their study (Rohrbach et al., 2012). In contrast to three-point bending used in this study, Rohrbach et al. (2012) used scanning acoustic microscopy to measure stiffness in bone and due to very high frequency rates applied, their stiffness measurements might have been affected by viscoelastic nature of the bone tissue. Similar to our results, Rohrbach et al. concluded that the elastic modulus along the bone cannot be correlated to BMD, yet they did not provide a suitable approach for accurately incorporating the heterogeneous distribution of the longitudinal elastic modulus in computational models of bone. Based on our findings, we propose that a location-based approach may be developed to account for variations of tissue-level elastic modulus in long bones.

Considering the femur to be subjected to bending loads, variations of the elastic modulus along the bone axis and in transverse cross-section of the bone, form an optimized structure capable of bearing different loads in everyday activities. Here, we reported the difference between the highest and lowest values of the elastic modulus to be approximately 79% (4.8-23.3 GPa) for femur-1 and 94% (1.6-28.4 GPa) for femur-2. We used two different bending fixtures to test each bone and part of the difference in the reported elastic moduli for the femurs can be explained in this way. It should be noted that the use of various fixtures had the same effect on all the samples tested by that method and therefore, this is not a major limitation to our conclusion on variations of the elastic modulus along the bovine femur. Although the same polynomial trend was obtained for both of the bones, the relation found for femur-1 could only predict part of the variations of the elastic modulus along the length of femur-2 ($R^2=0.61$, $P<0.05$). This is due to the fact that bones belonged to animals which could have different ages (both relatively young). In general, Haversian structure is not fully developed in bovine femur and results can be vastly different case by case. In any condition, the heterogeneity of the elastic modulus may find its origin in variations of bone structure at several hierarchical levels, including microporosity, osteonal density and collagen fibril orientation, rather than changes in the bone matrix mineralization alone. It has been shown that microstructural features affect the tissue level mechanical properties of bone in bovine samples (Rimnac et al., 1993; Hoc et al., 2006; Nobakhti et al., 2014). Further research is required to fully characterize the behavior of microstructural features along the long bones; this is beyond the scopes of current study.

To investigate the correlation of the elastic modulus with position along the bone, we used the mean of the data in each quadrant rather than applying all the data points to the analysis. This is justified due to the fact that the variability of measurements in each position is mainly coming from a size effect. The distribution of microstructures (osteons, pleixoform-lamellae) tends to be more homogeneous in larger samples and therefore, the standard deviation is lower in measuring their three-point bending elastic modulus. The small sample size was chosen such that multiple specimens could be harvested from each location with the trade-off of under-sampling the microstructures. From a statistical point of view and due to the existence of large number of data points, we have applied the k-means clustering technique (Duda et al., 2001) when doing the regression analysis. In this technique, objects belong to the same cluster if they are "close" according to a given measure. Each cluster of the points was then replaced by a single point, its mean value and the best-fit model was obtained between the elastic modulus and position along the femur. Our proposed location-based approach for estimation of longitudinal elastic modulus might only be applicable to long bones which are mainly subjected to bending loads and for other bones in body, the density-modulus relationships might still be the only alternative to form the heterogeneous FE models of bone tissue. Two bovine bones were tested in this analysis and the trends were similar in both cases. For establishing a more comprehensive relationship which accurately describes the elastic modulus based on position along the bovine femur however, many more bones with various age/gender characteristics should be investigated. Whether the behavior that we detected along the long axis of the bovine femur is also characteristic for human femora remains to be shown. Application of μCT for an

accurate approximation of the bone elastic modulus is restricted with this respect as μCT cannot predict the local variations of the bone microstructure. In this paper, we report a good correlation between the position along the bone and measured elastic modulus. Further investigation on a larger set of human samples is required to establish this link and to potentially define a “master” curve for cortical bone elastic modulus. Importantly, such an approach could in the future be used to improve heterogeneous property assignment of FE models based on μCT datasets, perhaps a general linear model including both local mineralization and position could improve the prediction of tissue level models.

Acknowledgment

We wish to acknowledge the μ-VIS X-Ray imaging center of the University of Southampton for provision of tomographic imaging facilities, supported by EPSRC grant EP-H01506X. We are also grateful to Dr. Maximilien Vanleene for providing MATLAB code to compute the mechanical properties of each sample from test data and Mr Habib Maddahi for help with preparing graphics for this paper.

Appendix A. Supporting information

Supplementary data associated with this article can be found in the online version at doi:10.1016/j.jmbbm.2017.03.021.

References

Atkinson, P.J., Weatherell, A.J., 1967. Variation in the density of the femoral diaphysis with age. J. Bone Jt. Surg. 49 (4), 781–788.
Cowper, G.R., 1966. The shear coefficient in Timoshenko's beam theory. J. Appl. Mech. 33 (2), 335–340.
Crawford, R.P., Cann, C.E., Keaveny, T.M., 2003a. Finite element models predict in vitro vertebral body compressive strength better than quantitative computed tomography. Bone 33 (4), 744–750.
Crawford, R.P., Rosenberg, W.S., Keaveny, T.M., 2003. Quantitative computed tomography-based finite element models of the human lumbar vertebral body: effect of element size on stiffness, damage, and fracture strength. J. Biomech. Eng. 125 (4), 434–438.
Cuppone, M., Seedhom, B.B., Berry, E., Ostell, A.E., 2004. The longitudinal Young’ s modulus of cortical bone in the midshaft of human femur and its correlation with CT scanning data. Calcif. Tissue Int. 74 (3), 302–309.
Duda, G.N., Heller, M., Albinger, J., Schulz, O., Schneider, E., Claes, L., 1998. Influence of muscle forces on femoral strain distribution. J. Biomech. 31 (9), 841–846.
Duda, R.O., Hart, P.E., Stork, D.G., 2001. Unsupervised Learning and Clustering, Ch. 10 in Pattern classification 2nd edition. Wiley, New York.
Edwards, W.B., Gillette, J.C., Thomas, J.M., Derrick, T.R., 2008. Internal femoral forces and moments during running: implications for stress fracture development. Clin. Biomech. 23 (10), 1269–1278.
Espinoza Orías, A.A., Deuerling, J.M., Landrigan, M.D., Renaud, J.E., Roeder, R.K., 2009. Anatomic variation in the elastic anisotropy of cortical bone tissue in the human femur. J. Mech. Behav. Biomed. Mater. 2 (3), 255–263.
Follet, H., Boivin, G., Rumelhart, C., Meunier, P.J., 2004. The degree of mineralization is a determinant of bone strength: a study on human calcanei. Bone 34 (5), 783–789.
Gere, J.M., Timoshenko, S.P., 1991. Mechanics of Materials. Chapman & Hall, London.
Hoc, T., Henry, L., Verdier, M., Aubry, D., Sedel, L., Meunier, A., 2006. Effect of microstructure on the mechanical properties of Haversian cortical bone. Bone 38 (4), 466–474.
Les, C.M., Stover, S.M., Keyak, J.H., 1997. The distribution of material properties in the equine third metacarpal bone serves to enhance sagittal bending. J. Biomech. 30 (4), 355–361.
Nobakhti, S., Limbert, G., Thurner, P.J., 2014. Cement lines and interlamellar areas in compact bone as strain amplifiers – Contributors to elasticity, fracture toughness and mechanotransduction. J. Mech. Behav. Biomed. Mater. 29, 235–251.
Oh, I., Harris, W.H., 1978. Proximal strain distribution in the loaded femur. An in vitro comparison of the distributions in the intact femur and after insertion of different hip-replacement femoral components. J. Bone Jt. Surg. 60 (1), 75–85.
Poelert, S., Valstar, E., Weinans, H., Amir, A., 2012. Patient-specific finite element modeling of bones. Proc. Inst. Mech. Eng. H J. Eng. Med 227 (4), 464–478.
Polgar, K., Gill, H.S., Viceconti, M., Murray, D.W., 2003. Strain distribution within the human femur due to physiological and simplied loading: finite element analysis using the muscle standardized femur model. Proc. Inst. Mech. Eng. H J. Eng. Med. 217 (3), 173–189.
Rantalainen, T., Nikander, R., Daly, R.M., Heinonen, A., Sievänen, H., 2011. Exercise loading and cortical bone distribution at the tibial shaft. Bone 48 (4), 786–791.
Rho, J.Y., Scottish, T., Hospital, R., 1995. Relations of mechanical properties CT numbers in human bone. Med. Eng. Phys. 17 (5), 347–355.
Rimnac, C.M., Petko, A.A., Santner, T.J., Wright, T.M., 1993. The effect of temperature, stress and microstructure on the creep of compact bovine bone. J. Biomech. 26 (3), 219–221.
Rohrbach, D., Lakshmanan, S., Langer, M., Gerisch, A., Grimal, Q., Laugier, P., Raum, K., 2012. Spatial distribution of tissue level properties in a human femoral cortical bone. J. Biomech. 45 (13), 2264–2270.
Schneider, U., Pedroni, E., Lomax, A., 1996. The calibration of CT Hounsfield units for radiotherapy treatment planning. Phys. Med. Biol. 41 (1), 111–124.
Shahar, R., Banks-sills, L., Eliasy, R., 2003. Stress and strain distribution in the intact canine femur: finite element analysis. Med. Eng. Phys. 25 (5), 387–395.
Szabo, M.E., Taylor, M., Thurner, P.J., 2011. Mechanical properties of single bovine trabeculae are unaffected by strain rate. J. Biomech. 44 (5), 962–967.
Taddei, F., Martelli, S., Reggiani, B., Cristofolini, L., Viceconti, M., 2006. Finite-element modeling of bones from CT Data: sensitivity to geometry and material uncertainties. IEEE Trans. Biomed. Eng. 53 (11), 2194–2200.
Wagner, D.W., Lindsey, D.P., Beaupre, G.S., 2011. Deriving tissue density and elastic modulus from microCT bone scans. Bone 49 (5), 931–938.
Wolff, J., 1892. Das Gesetz der Transformation der Knochen. A. Hirchwild, Berlin.